NeuroImage: Clinical 44 (2024) 103686

Contents lists available at ScienceDirect

NeuroImage: Clinical

journal homepage: www.elsevier.com/locate/ynicl

Altered brain complexity in first-episode antipsychotic-naïve patients with schizophrenia: A whole-brain voxel-wise study

Naici Liu [a,1], Rebekka Lencer [b,c,1], Christina Andreou [b], Mihai Avram [b], Heinz Handels [d,e], Wenjing Zhang [a], Sun Hui [a], Chengmin Yang [a], Stefan Borgwardt [b], John A. Sweeney [f], Su Lui [a,*], Alexandra I. Korda [b,*]

[a] Department of Radiology, and Functional and Molecular Imaging Key Laboratory of Sichuan Province, West China Hospital of Sichuan University, Chengdu, China
[b] Department of Psychiatry and Psychotherapy, and Center for Brain, Behavior and Metabolism, University of Lübeck, Lübeck, Germany
[c] Institute for Translational Psychiatry and Otto-Creutzfeldt Center for Behavioral and Cognitive Neuroscience, University of Münster, Münster, Germany
[d] Institute of Medical Informatics, University of Lübeck, Lübeck, Germany
[e] German Research Center for Artificial Intelligence, Lübeck, Germany
[f] Psychiatry & Behavioral Neuroscience, College of Medicine, University of Cincinnati, Cincinnati, USA

ARTICLE INFO

Keywords:
Schizophrenia
Non-linear dynamic model
Cortical topology
Largest Lyapunov exponent
Brain complexity

ABSTRACT

Background: Measures of cortical topology are believed to characterize large-scale cortical networks. Previous studies used region of interest (ROI)-based approaches with predefined templates that limit analyses to linear pair-wise interactions between regions. As cortical topology is inherently complex, a non-linear dynamic model that measures the brain complexity at the voxel level is suggested to characterize topological complexities of brain regions and cortical folding.

Methods: T1-weighted brain images of 150 first-episode antipsychotic-naïve schizophrenia (FES) patients and 161 healthy comparison participants (HC) were examined. The Chaos analysis approach was applied to detect alterations in brain structural complexity using the largest Lyapunov exponent (Lambda) as the key measure. Then, the Lambda spatial series was mapped in the frequency domain using the correlation of the Morlet wavelet to reflect cortical folding complexity.

Results: A widespread voxel-wise decrease in Lambda values in space and frequency domains was observed in FES, especially in frontal, parietal, temporal, limbic, basal ganglia, thalamic, and cerebellar regions. The widespread decrease indicates a general loss of brain topological complexity and cortical folding. An additional pattern of increased Lambda values in certain regions highlights the redistribution of complexity measures in schizophrenia at an early stage with potential progression as the illness advances. Strong correlations were found between the duration of untreated psychosis and Lambda values related to the cerebellum, temporal, and occipital gyri.

Conclusions: Our findings support the notion that defining brain complexity by non-linear dynamic analyses offers a novel approach for identifying structural brain alterations related to the early stages of schizophrenia.

1. Introduction

Schizophrenia is suggested to result from irregularities within distributed neural networks rather than dysfunctions of single distinct brain regions (van den Heuvel and Fornito, 2014; Jiang et al., 2022). Measures of brain topology quantified large-scale cortical networks (He and Evans, 2010; Fornito et al., 2012; Zhang et al., 2023), demonstrating reduced structural integrity of fronto-parietal and salience networks (including dorsal anterior cingulate and fronto-insular cortices) in patients with schizophrenia (Spreng et al., 2019).

Previous large-scale cortical network studies of structural topological alternations in schizophrenia mainly investigated the covariation in

* Corresponding authors at: Department of Psychiatry and Psychotherapy, and Center for Brain, Behavior and Metabolism, University of Lübeck, Lübeck, Germany (Alexandra I. Korda). Department of Radiology, and Functional and Molecular Imaging Key Laboratory of Sichuan Province, West China Hospital of Sichuan University, Chengdu, China (Su Lui).
E-mail addresses: lusuwcums@tom.com (S. Lui), alexandra.korda@uni-luebeck.de (A.I. Korda).
[1] Equal contributions.

https://doi.org/10.1016/j.nicl.2024.103686
Received 4 June 2024; Received in revised form 7 October 2024; Accepted 7 October 2024
Available online 10 October 2024

gray matter volume (Liu et al., 2021), cortical thickness (Zhang et al., 2020), or cortical gyrification (Palaniyappan et al., 2015) using graph theory. This approach uses connectivity matrices based on correlation degrees between defined brain regions to investigate interactions between paired regions (Yu et al., 2018). However, region of interest (ROI)-based approaches with a predefined template limit investigations to linear pair-wise interactions between brain regions, requiring a template-based definition of such regions (van den Heuvel et al., 2008). As individual brain regions do not inevitably represent the minimum functional unit of the brain, voxel-wise approaches are more promising to match inherently complex cortical topology (Tian et al., 2019; Kim et al., 2015).

Furthermore, a non-linear dynamic model that represents the multiplex brain structure using complexity measures, rather than linear pair-wise correlations (Fernandez et al., 2013) appears better suited for characterizing complex data in biological neural systems (Pham et al., 2015). In line with this, it has been suggested that nonlinear methods may better explain brain structural alterations as observed in schizophrenia (Breakspear, 2006). Concerning the application of Chaos theory, the largest Lyapunov exponent (Lambda [λ]) derived from a Lyapunov exponent equation is well-established as a measure of complexity in dynamical systems (Kim et al., 2000). In this model, the Lambda value quantifies the divergence of small distances across voxel locations, serving as a quantitative indicator of geometry, curvature, and, consequently, the topological complexity of the evaluated brain regions (Korda et al., 2022). That is, the complexity of brain regions in patients can be investigated through the collective interactions between multiple voxel intensities at different locations. Moreover, continuous wavelet transformations (CWT) can decompose Lambda series into their frequency ("multiscale") components, representing the structure relief of the brain and enabling the quantification of the cortical folding complexity (Korda et al., 2022). For instance, increased cortical structural complexity has been reported in patients with first-episode psychosis in the temporal pole, right posterior cingulate gyrus, and lingual and fusiform gyri when compared with healthy comparison participants (HC), a finding which might contribute to the identification of structural biomarkers (Korda et al., 2022).

In the present study, the topological complexity of brain regions was compared between 150 antipsychotic-naïve patients with first-episode schizophrenia (FES) and 161 HC by estimating Lambda values across the whole brain (Chen and Pham, 2013). A voxel-wise approach was used to allow for the template-free examination of both inter-regional as well as intra-regional interactions at the whole-brain level (van den Heuvel et al., 2008). Additionally, the complexity of cortical folding was estimated to realize the visualization of the structural roughness of Lambda series (Korda et al., 2022). The associations between clinical symptom severity and topological complexities of both brain and cortical folding were investigated as well. Results were compared with findings from voxel-based morphometry (VBM) and gyrification indices (GI) using established standard procedures. We hypothesized that 1) reductions in brain and cortical folding complexities would be observed in patients with FES, as schizophrenia has been proposed to involve potential deficits in cortical maturation (Li et al., 2016); 2) the current voxel-vise approach would be more sensitive in detecting cortical alterations than conventional VBM and surfaced-based morphometry (SBM) methods.

2. Methods and materials

2.1. Participants

One hundred and fifty antipsychotic-naïve patients with FES were recruited from West China Hospital in Chengdu, China. Diagnostic evaluations were conducted using the Structured Interview for DSM-IV Axis I Disorders (SCID) (First, 2005) to establish standardized criteria for clinical diagnoses. The severity of symptom expression covering seven days before testing was assessed using the Positive and Negative Syndrome Scale (PANSS) (Kay et al., 1987). In addition to the positive and negative scales and global psychopathology subscores, we also determined subscores for thought disturbances (comprising P2 + P3 + P5 + G9), activation (comprising P4 + G4 + G5), paranoid syndrome (comprising P6 + P7 + G8), depression (comprising G1 + G2 + G3 + G6), anergia (comprising N1 + N2 + G7 + G10), and impulsive aggression (P4 + P7 + G6 + S1 + S2 + S3) according to the original six-factor model of the PANSS (Gladsjo et al., 2004) Furthermore, the duration of untreated psychosis (DUP) was determined by the Nottingham Onset Schedule (Singh et al., 2005). HC with similar demographic characteristics were recruited through website advertisements (Table 1). The non-patient version of the SCID (First, 2002) was administered to the HC group to confirm the lifetime absence of psychotic, mood, and substance use disorders. All participants were right-handed and assessed based on the Annett Handedness Scale (Dragovic and Hammond, 2007) and of Han ancestry. Exclusion criteria for both groups included a history of traumatic brain injury or significant systemic or neurological disorders. The study protocol was approved by the research ethics committee of West China Hospital of Sichuan University. Written informed consent was obtained from all study participants.

2.2. MRI data acquisition

MRI data were collected on a 3-T scanner (EXCITE, General Electric, Milwaukee). To minimize the subject's head motion, the head coil and earplugs were employed. High-resolution anatomical T1-weighted images were acquired with a three-dimensional spoiled gradient sequence: TR = 8.5 ms, TE = 3.5 ms, TI = 400 ms, flip angle = 12°, with a 240 × 240 matrix over a field of view of 240 × 240 mm resulting in 156 axial slices of 1 mm thickness. All scans were reviewed by an experienced neuroradiologist to rule out gross brain abnormalities.

Table 1
Demographic and clinical characteristics of the study participants.

	FES (n = 150)		HC (n = 161)		t value	p value
	mean	SD	mean	SD		
Age (years)	23.5	7.1	24.7	7	−1.50	0.135
Education (years)	12.2	3.0	13.1	3.1	−2.72	0.007
DUP (months)	9.1	15.1				
Sex					χ^2	**p value**
Female (N)	88		82		1.88	0.171
Male (N)	62		79			
PANSS						
Total scores	90.08	16.88				
The sum of positive symptoms	25.02	6.22				
The sum of negative symptoms	18.43	7.87				
The sum of global psychopathology	46.63	9.38				
The six-factor model of PANSS						
Thought disturbances	14.00	3.89				
Activation	9.25	3.36				
Paranoid syndrome	10.33	2.82				
Depression	8.55	4.09				
Anergia	8.64	4.35				
Impulsive aggression	16.13	5.16				

Abbreviations: DUP, duration of untreated psychosis; FES, first-episode antipsychotic-naïve schizophrenia; HC, healthy comparison participants; PANSS, Positive and Negative Syndrome Scale.

2.3. MRI data preprocessing

The structural image preprocessing was carried out using the Computational Anatomy Toolbox (CAT) (Fornito et al., 2009) which is an extension of the Statistical Parametric Mapping software (SPM) 12 based on MATLAB R2014b. The analysis pipeline was also followed in our previous study (Korda et al., 2022) and presented here briefly. First, T1-weighted images were segmented into gray matter (GM), white

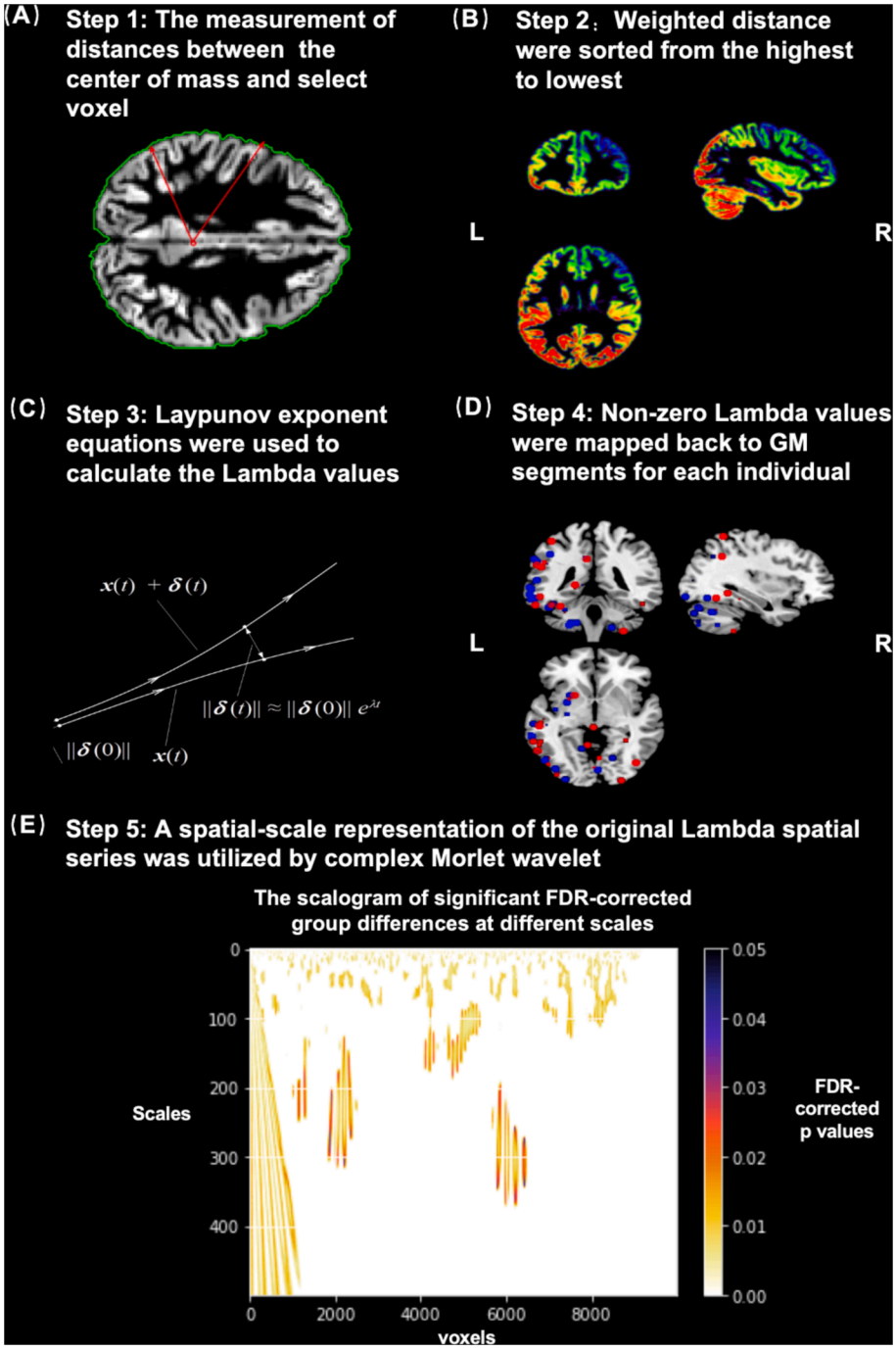

Fig. 1. Flowchart of the Chaos analysis and Continuous Wavelet transformation. (A) step 1: the distances between the center of mass and all voxels were measured based on the modulated and normalized GM segment images, (B) step 2: weighted distances (distance in mm × voxel intensity) were obtained to capture geometric changes in brain regions and were sorted from the highest to lowest, higher weighted distances are indicated by red/warm color and lower weighted distance are indicated by blue/cold color. Then the top 10,000 non-zero voxels were retained to estimate Lambda values, (C) step 3: Lyapunov exponent equations and explanation of the divergence of the points in a state-space, (D) step 4: non-zero Lambda values were mapped back to GM segments for each individual. Representations of the mean non-zero Lambda values of FES (red) and HC (blue) at the group level, (E) step 5: a spatial-scale representation of the original Lambda spatial series of the 10,000 selected voxels was utilized. The Scalogram showed significant FDR-corrected group differences at different scales (0–500). Selected top 10,000 non-zero voxels are represented on the x-axis and scales on the y-axis. Each value in the scalogram represents the correlation of the Lambda series with the Morlet wavelet on the respective voxel and scale. The colors represent the correlation with the Morlet wavelet with deep purple color corresponding to larger and white color corresponding to smaller FDR-corrected p-values. All voxels had significant FDR-corrected p values. Abbreviations: GM, gray matter; FDR, false discovery rate; L, left; R, right.

matter (WM), and cerebrospinal fluid (CSF) using a standard segmentation model in CAT12 (Spalthoff et al., 2018). Second, a hidden Markov Random Field model was applied to obtain a higher signal-to-noise ratio of the final tissue probability maps (Cuadra et al., 2005). Third, the filter strength involved an automatic assessment based on estimating the residual noise in each image. Fourth, the original voxels underwent projection into new locations in the warped images, ensuring the preservation of tissue volume within each voxel. This preservation process was achieved through a combination of affine transformation (global scaling) and non-linear warping (local volume change). Finally, the segmented GM, WM, and CSF maps were normalized to the Montreal Neurological Institute (MNI) space and modulated. Each voxel with an isotropic voxel size of 1.5 mm was used for the extraction of the spatial series.

2.4. Chaos analysis and topologic complexity of cortical folding

A flowchart depicting the principles of the Chaos analysis is shown in Fig. 1. The center of mass of the modulated and normalized GM segments was first obtained by the function named "center of Mass" in MATLAB R2014b which could find the gray-level-weighted center of mass of an N-dimensional numerical array. The weighted distance of the GM center of mass with the voxel intensities (distance in mm × voxel intensity) was calculated to capture geometric changes in brain regions. The weighted distances were sorted from the highest to lowest. The top-weighted distances correspond to voxels that either belonged to the cortical surface or were slightly close to the center mass of GM. The highest 10,000 voxels were ultimately left to maintain the balance between computational cost and reserving the topological differences between groups. Then, the highest 10,000 voxels accounting for 2 % of the non-zero voxels in the GM segments were extracted as the spatial series to reconstruct the matrix of the state space and to estimate the Lambda value (Rosenstein et al., 1993; Korda et al., 2018).

An approach developed by Rosenstein was applied to obtain Lambda values (Rosenstein et al., 1993). This approach was appropriate for small datasets and was robust to the embedding dimension, reconstruction delay, and noise (Rand and Young, 1981). The detailed procedure of this method was described in our previous study (Korda et al., 2022). Briefly, positive Lambda values are known to depict the sensitive dependence on initial conditions in a dynamical system. According to the theory of Takens (Rand and Young, 1981), the trajectory of a system's attractor, whose states evolve with spatial location over a state-space and predict the interactions between multiple voxel intensities, can be described by a matrix X. Thus, in a finite state-spatial, Takens's Theorem is not restricted to time series. We can let xi denote the spatial-series of the path-free sorted distances extracted from the brain's sMRI. Assuming the given spatial series provides an observation of a dynamical system where the parameter time is replaced by the voxel intensity and distance from the center of the mass combined. Then, the Lambda could be considered as a feature describing structural aspects of the cortex.

Lambda value quantified the divergence of small distances across voxel locations, serving as a quantitative indicator of the topological complexity of the evaluated brain regions (Korda et al., 2022). That is, the complexity of brain regions in patients can be investigated by the collective interactions over locations between multiple voxel intensities. To obtain the location, Lambda values were mapped back to GM segments for each individual using the stored coordinates of the weighted distances of each voxel. Lambda values of voxels that were not selected as the top-weighted voxels were set to 0.

2.5. Continuous wavelet transformation

The pipeline of the continuous wavelet transformation (CWT) followed a previous report by our group (Korda et al., 2022). In short, the CWT utilizes a fully scalable modulated window, offering a robust solution to the windowing function selection challenge in frequency-related (scale-related) signal processing methodologies (Korda et al., 2022). In the present investigation, the CWT was applied to decompose the Lambda series into frequency components for feature extraction. The CWT utilized the complex Morlet wavelet as its fundamental function to produce a spatial-scale representation of the original Lambda spatial series, displayed as a "scalogram" plane (Korda et al., 2022). That is, the CWT of a one-dimensional series has two-dimensional outputs of a scalogram that contains geometrical points and scales (Korda et al., 2022). Within this scalogram plane, each value (referred to as a wavelet coefficient) signifies the degree of correlation between the Lambda series and the Morlet wavelet at specific geometrical point-scale pairs. This approach facilitated the quantification of cortical folding complexity by extracting statistical features representing the structural relief of brain geometry, which were subsequently computed in the spatial domain.

2.6. Statistical analysis

Lambda images were loaded in MATLAB R2014b using a two-sample *t*-test to obtain group differences between FES and HC at the voxel level. P-values of the 10,000 selected top-weighted voxels were corrected with a false discovery rate (FDR) to correct for multiple comparisons. An FDR-corrected p-value (two-tailed) < 0.05 was considered statistically significant. FDR-corrected p values were mapped back to GM segments and allocated to 116 regions based on the AAL templates in MRICron (https://www.nitrc.org/projects/mricron/). The corresponding brain regions with the number of non-zero voxels in each region and mean Lambda values of non-zero voxels were presented in Table 2. Raw test statistics, p-values, and coordinates of significant voxels were not provided in the results part owing to their large number. The presented coordinates are restricted to those brain regions with both increased and decreased measures of brain complexity.

Regarding the Lambda values at different scales, group comparisons with significant FDR-corrected p values were represented using the scalograms from 0 to 500 (Fig. 1E). The 400 scales were found to provide the most adequate representation for each group and were selected for further two-sample t-tests to compare the group differences with the significance level set at $p < 0.05$ (FDR corrected). A surface overlay of the mean correlations between the Lambda values and the Morlet wavelet was applied to represent the statistically significant differences in 400 scales by using CAT12 (Fig. 4A and B). As above, only brain regions with both increased and decreased measures of cortical complexity were presented with coordinates.

After group comparisons, Lambda values in space and frequency domains showing significant group differences were further used to identify associations with clinical scores by conducting partial correlation analyses with age and sex as covariates of no interest.

2.7. Voxel-based morphometry analysis

For exploratory purposes, VBM analyses were performed to identify gray matter volume differences between groups. The modulated and warped GM segments were smoothed with an 8 mm full-width at half maximum (FWHM) Gaussian Kernel. After spatial pre-processing, the smoothed, modulated, normalized GM segments were used for statistical analysis in the context of the general linear model in the SPM12 toolbox. Voxel-wise two-sample t-tests were performed using age and sex as covariates. The threshold was set at $p < 0.05$ corrected by the family-wise error rate (FWE). A contiguous cluster of at least 30 voxels was accepted as significant. The significant findings were visualized using MRICron.

2.8. Gyrification index analysis

Additionally, SBM pre-processing and analyses were performed using the default CAT12 pipeline which has been used in previous studies of patients with schizophrenia (Spalthoff et al., 2018). A

Table 2
Brain regions showing FDR-corrected decreased brain complexity in FES compared with HC by applying two sample t-tests on Lambda values.

Brain regions	Number of voxels	Number of non-zero voxels	Fraction of non-zero voxels	Mean Lambda values in space of non-zero voxels
Precentral L	28,174	565	0.020	0.000161
Frontal Sup Orb L	7654	89	0.012	0.000105
Frontal Mid L	38,722	1	<0.001	0.000138
Frontal Inf Tri L	20,104	54	0.003	0.000080
Rolandic Oper L	7939	7	0.001	0.000189
Rectus L	6864	163	0.024	0.000156
Insula L	15,025	836	0.056	0.000053
Cingulum Mid L	15,512	292	0.019	0.000101
Cingulum Post L	3715	205	0.055	0.000504
Hippocampus L	7469	9	0.001	0.000110
Parahippocampal L	7891	112	0.014	0.000209
Calcarine L	18,157	1941	0.107	0.000102
Calcarine R	14,885	923	0.062	0.000124
Cuneus L	12,133	779	0.064	0.000121
Cuneus R	11,323	592	0.052	0.000107
Lingual L	16,932	1308	0.077	0.000104
Lingual R	18,450	1372	0.074	0.000144
Occipital Sup L	10,791	307	0.028	0.000140
Occipital Sup R	11,149	96	0.009	0.000172
Occipital Mid L	25,989	3751	0.144	0.000177
Occipital Mid R	16,512	181	0.011	0.000159
Occipital Inf L	7536	1779	0.236	0.000131
Occipital Inf R	7929	710	0.090	0.000179
Fusiform L	18,333	3152	0.172	0.000192
Fusiform R	20,227	913	0.045	0.000166
Postcentral L	31,053	649	0.021	0.000106
Parietal Sup L	16,519	28	0.002	0.000223
Parietal Sup R	17,554	358	0.020	0.000118
Parietal Inf L	19,447	691	0.036	0.000186
SupraMarginal L	9907	1383	0.140	0.000144
Angular L	9313	688	0.074	0.000164
Angular R	14,009	515	0.037	0.000121
Precuneus L	28,358	1599	0.056	0.000271
Precuneus R	26,083	594	0.023	0.000138
Paracentral Lobule R	6693	540	0.081	0.000155
Putamen L	7942	1348	0.170	0.000279
Pallidum L	2285	198	0.087	0.000156
Thalamus L	8700	837	0.096	0.000268
Thalamus R	8399	567	0.068	0.000205
Temporal Sup L	18,307	1737	0.095	0.000103
Temporal Pole Sup L	10,228	32	0.003	0.000103
Temporal Mid L	39,353	5754	0.146	0.000154
Temporal Mid R	35,484	32	0.001	0.000163
Temporal Pole Mid L	5984	9	0.002	0.000175
Temporal Inf L	25,647	4106	0.160	0.000351
Temporal Inf R	28,468	2078	0.073	0.000175
Cerebellum Crus1 L	20,667	2818	0.136	0.000133
Cerebellum Crus1 R	21,017	1469	0.070	0.000138
Cerebellum Crus2 L	15,216	2175	0.143	0.000125
Cerebellum Crus2 R	17,038	886	0.052	0.000165
Cerebellum 3 R	1600	1	0.001	0.000123
Cerebellum 4 5 L	9034	687	0.076	0.000026
Cerebellum 4 5 R	6763	523	0.077	0.000085
Cerebellum 6 L	13,672	3472	0.254	0.000299
Cerebellum 6 R	14,362	1177	0.082	0.000131
Cerebellum 7b L	4639	1055	0.227	0.000154
Cerebellum 7b R	4230	146	0.035	0.000210
Cerebellum 8 L	15,090	1099	0.073	0.000192
Cerebellum 8 R	18,345	1504	0.082	0.000143
Cerebellum 9 L	6924	184	0.027	0.000137
Cerebellum 9 R	6462	179	0.028	0.000124
Vermis 4 5	5324	32	0.006	0.000094
Vermis 7	1564	5	0.003	0.000087
Vermis 8	1940	690	0.356	0.000089
Vermis 9	1367	254	0.186	0.000206
Vermis 10	874	158	0.181	0.000168

Abbreviations: Inf, inferior; L, left; Mid, middle; Oper, operculum; Orb, orbital part; Post, posterior; R, right; Sup, superior; Tri, triangular part.

gyrification index, one of the SBM parameters, was extracted with the CAT12 toolbox (Dahnke et al., 2013) based on the absolute mean curvature of the cortex (Luders et al., 2006). A Gaussian kernel of 20 mm was applied to smooth the gyrification images. The statistical analysis was performed in CAT12 using a general linear model with a two-sample *t*-test design. Results were considered significant at the cluster-level FWE-corrected $p < 0.05$ for multiple comparisons. The significant findings were visualized using CAT12.

3. Results

3.1. Demographic characteristics

A total of 150 antipsychotic-naïve patients with FES (88 females, 62 males; mean age of entire sample: 23.5 ± 7.1 years, range: 16–44 years; DUP: 9.1 ± 15.1 months; education: 12.3 ± 2.8 years) and 161 HC matched by age and sex (82 females, 79 males; mean age: 24.7 ± 7.0 years, range: 16–45 years; education: 13.1 ± 3.1 years) was included in this study (Table 1). Notably, the HC group had a significantly higher educational level than the patient group.

3.2. The distribution of Lambda values

As laid out above, the distribution of Lambda reflects the topological complexity of the brain. In both groups, Lambda distribution patterns were predominately found related to the left hemisphere (Fig. 1) with Lambda values differing between both groups indicating brain complexity alterations in patients.

3.3. Altered brain complexity in patients with schizophrenia and its association with clinical scores

Specifically, patients predominately showed decreased topological complexity in left frontal, left limbic, left basal ganglia regions and bilateral occipital, parietal, temporal, thalamic, and cerebellar regions ($p < 0.05$, FDR-corrected, Table 2, Fig. 2). Interestingly, some voxels among these regions (i.e. left middle occipital gyrus, left fusiform gyrus, left thalamus, left temporal gyrus, and left cerebellum) also presented increased topological complexity in patients compared with HC ($p < 0.05$, FDR-corrected, Table S1).

Partial correlation analyses with age and sex as covariates showed correlations between brain complexity and DUP in several brain regions in the patient group: longer DUP was associated with higher complexity in the cerebellum, temporal, and occipital gyri. We also observed correlations between brain complexity and clinical symptoms. To be specific, stronger PANSS negative symptom expression was associated with higher complexity in the cerebellum, temporal, and occipital gyri. Meanwhile, stronger expression of anergia was associated with higher complexity in the left cerebellum crus 1 (Table 3, Fig. 3).

3.4. Altered cortical folding complexity in patients with schizophrenia and associations with clinical scores

Significant group differences were observed in several frequency

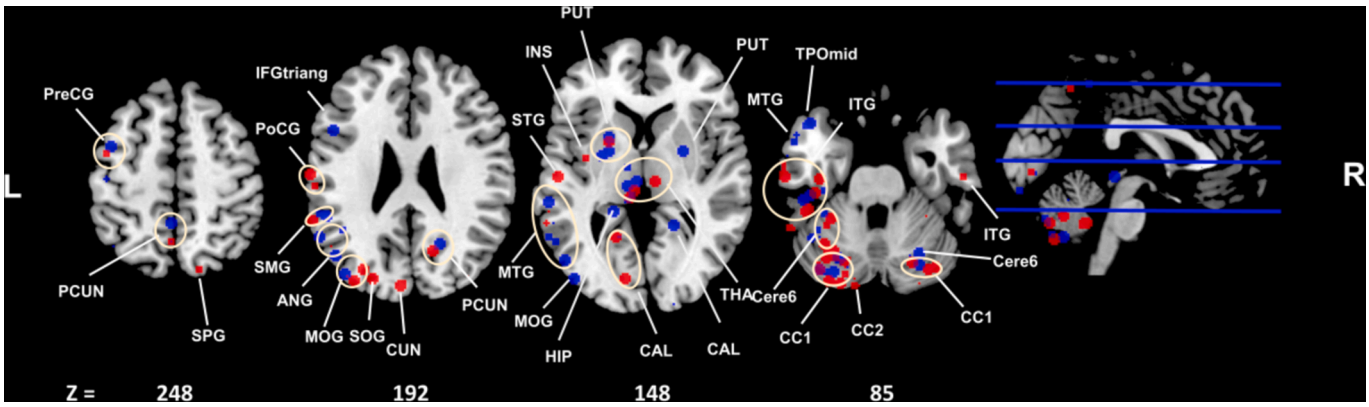

Fig. 2. Brain regions showing significant FDR corrected group differences in Lambda values indicating both higher and lower complexity in FES compared with HC. Blue spots represent FES while red spots represent HC (FWHM = 6 mm). The horizontal blue lines in the right part of the figure indicate the axial slice locations. The spots in the same brain area are circled by yellow lines. Abbreviations: ANG, angular gyrus; CAL, calcarine fissure and surrounding cortex; CC1, cerebellum crus 1; CC2, cerebellum crus 2; Cere6, cerebellum 6; CUN, cuneus; IFGtriang, triangular part of inferior frontal gyrus; INS, insula; ITG, inferior temporal gyrus; L, left; MOG, middle occipital gyrus; MTG, middle temporal gyrus; PCUN, Precuneus; PreCG, precentral gyrus; PUT, putamen; R, right; SMG, Supramargnial gyrus; SOG, superior occipital gyrus; SPG, superior parietal gyrus; THA, thalamus.

Table 3
Partial correlations between brain complexity and DUP/clinical symptoms defined by PANSS in FES using age and sex as covariates.

	Brain region	r value	FDR-corrected p value
DUP	Temporal Mid L	0.773	<0.00001
	Temporal Mid R	0.749	<0.00001
	Temporal Inf L	0.749	<0.00001
	Occipital Mid L	0.749	<0.00001
	Cerebellum Crus 1 L	0.749	<0.00001
	Cerebellum Crus 2 L	0.596	<0.00001
	Cerebellum Crus 2 R	0.749	<0.00001
	Cerebellum 6 L	0.733	<0.00001
	Cerebellum 8 L	0.749	<0.00001
	Cerebellum 8 R	0.679	<0.00001
Anergia Syndrome	Cerebellum Crus 1 L	0.302	0.04706
Negative Symptoms	Temporal Mid L	0.349	0.03529
	Temporal Mid R	0.337	0.01176
	Temporal Inf L	0.337	0.01569
	Occipital Mid L	0.337	0.00784
	Cerebellum Crus 1 L	0.337	0.04314
	Cerebellum 6 L	0.337	0.01176
	Cerebellum 8 R	0.330	0.01176

Abbreviations: Inf, inferior; L, left; Mid, middle; R, right.

scales (0–500). In 400 scales the number of the FDR corrected p-values (<0.05) was higher than in other scales and were finally selected for further analysis. This indicates that low frequencies (high scales) were more prominent in patients reflecting a smoother divergence of voxels in the spatial series (Fig. 4). Specifically, patients showed decreased topological complexity of cortical folding in left frontal and bilateral limbic regions, basal ganglia, as well as occipital, parietal, temporal, thalamic, and cerebellar regions ($p < 0.05$, FDR-corrected, Table 4). Meanwhile, some voxels among these regions (e.g., left parietal lobe, left precentral gyrus, right cuneus gyrus, bilateral superior occipital gyrus, and bilateral cerebellum) also presented increased topological complexity of cortical folding in patients compared with HC ($p < 0.05$, FDR-corrected, Table S2).

Partial correlation analysis with age and sex as covariates showed that higher PANSS depression subscores and lower paranoid syndrome subscores were associated with higher complexity of cortical folding in the right thalamus ($r = 0.3713$, FDR p-value ≤ 0.05) and left middle occipital gyrus ($r = -0.3596$, FDR p-value ≤ 0.05) in patients compared with HC, respectively (Fig. 5).

3.5. Voxel-based morphometry analysis

To compare the results conducted by the non-linear dynamic model with the results obtained by the conventional morphometric method, VBM analyses were performed to identify gray matter volume differences between groups. Patients with FES showed significantly decreased gray matter volume than HC related to the left parahippocampus, left cerebellum crus 1, and right lingual gyrus (Table S3, Fig. S1). No increased gray matter volume was observed in any regions in the patient group when compared with the healthy group.

3.6. Surfaced-based morphometry analysis

For a similar exploratory purpose as above, SBM analyses were further conducted to figure out group differences in gray matter gyrification. Patients with FES showed a significant hypo-gyrification pattern than HC in the left middle temporal and right superior temporal gyri (Table S4, Fig. S2). No hyper-gyrification pattern was observed in any regions when compared with the healthy group.

4. Discussion

To identify alterations of topological brain complexity and cortical folding in antipsychotic-naïve patients with FES, we applied the Chaos analysis using Lambda values and Lambda values in the frequency domain as key measures. Our main findings demonstrated a widespread voxel-wise decrease of Lambda values and their components at 400 scales, indicating a general reduction of topological brain and cortical folding complexities in patients at an early stage of this severe mental disorder. Most importantly, we identified associations between brain complexity and DUP/ psychopathological symptoms (anergia and negative symptoms) on the one hand, and associations between cortical folding complexity and psychopathological symptoms (depression and paranoid syndrome) on the other hand.

Generally, we found distributions of Lambda values, with higher Lambda values representing higher brain complexity, mainly located in the left occipital and temporal regions and cerebellum in both FES and HC groups. These findings were consistent with previous reports about human brain lateralization (left–right asymmetry) representing a substantial feature of human brain organization (Schijven et al., 2023) shaped by neurodevelopmental processes (Koelkebeck et al., 2014; Sha et al., 2021). In line with this, the exhibition of a general left-greater-than-right asymmetry had been associated with unequal development of diverse brain regions (e.g., language and right-handedness) mostly in

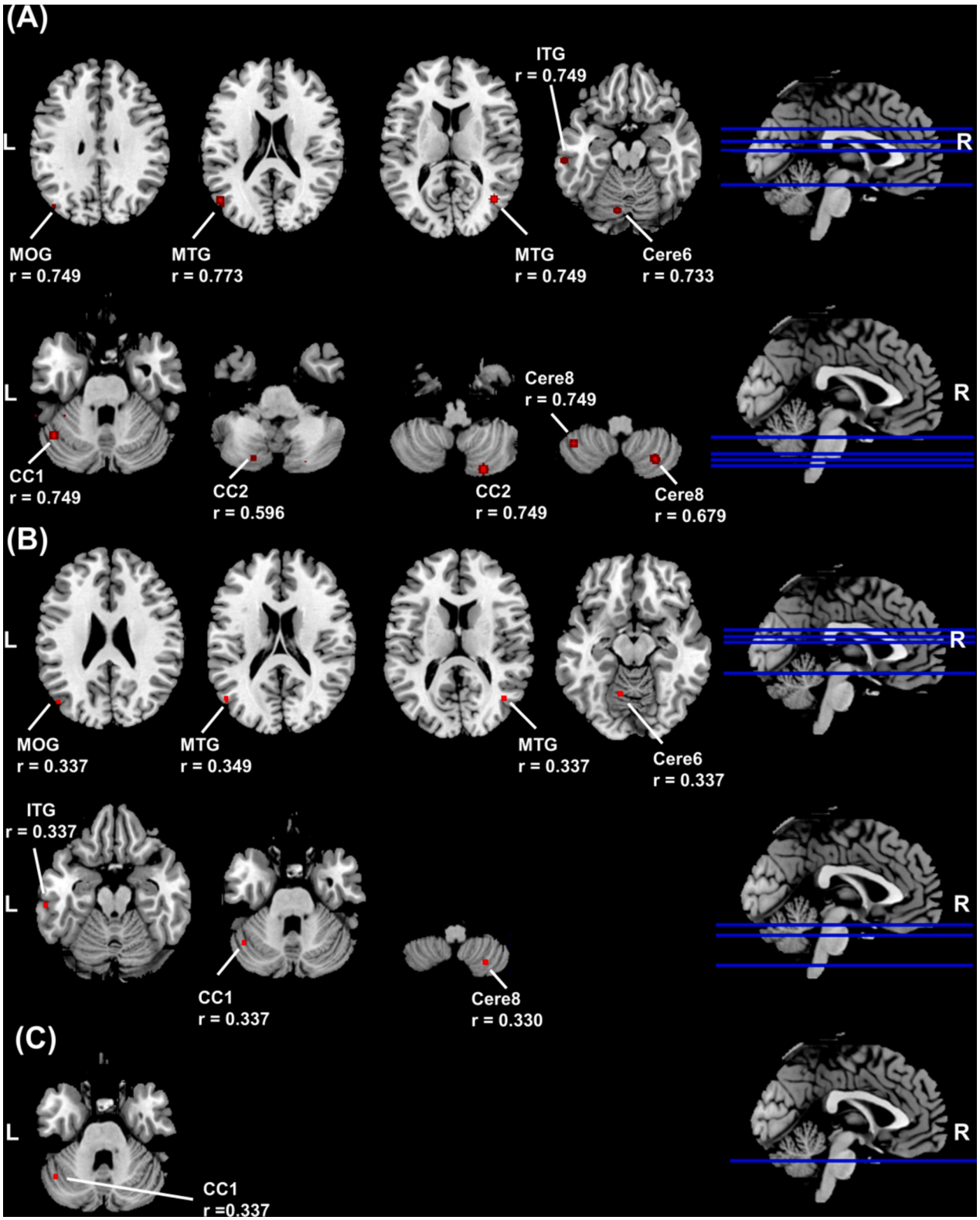

Fig. 3. Correlations between brain complexity and (A) DUP, (B) negative syndrome, and (C) anergia subscores in FES. The red spots indicate positive correlations (FWHM = 6 mm). The horizontal blue lines in the right part of the figure indicate the axial slice locations. Abbreviations: CC1, cerebellum crus1; CC2, cerebellum crus2; Cere6, cerebellum 6; Cere8, cerebellum 8; ITG, inferior temporal gyrus; L, left; MOG, middle occipital gyrus; MTG, middle temporal gyrus; R, right.

HC (Kong et al., 2018; Toga and Thompson, 2003). Thus, the general pattern of Lambda distribution found in both groups supported a model of Lambda representing reliable measures of topological brain complexities.

Second, the widespread voxel-wise decrease in Lambda values observed in first-episode patients indicated an extensive brain complexity decrease in the left hemisphere, with some additional brain regions showing decreased complexity also in the right hemisphere. This was consistent with previous reports showing decreased brain structural complexity in schizophrenia patients compared with HC (Squarcina

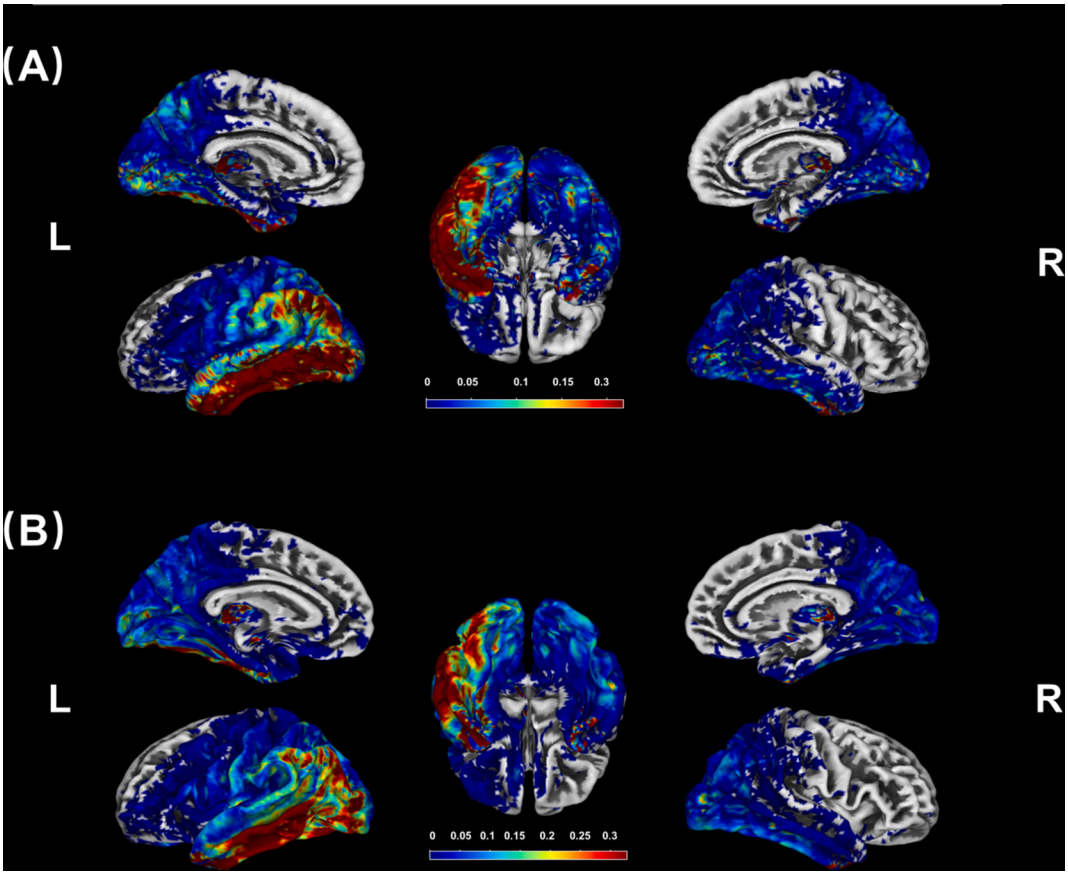

Fig. 4. Correlations of the Lambda values with the Morlet wavelet in voxels with statistically significant FDR-corrected differences for 400 scales were overlaid to (A) FES and (B) HC. The color scale represents the range of the correlation, higher (lower) correlations are indicated by red/warm (blue/cold) color and represent smooth (sharp) cortical folding. Abbreviations: L, left; R, right.

et al., 2015). Decreased Lambda values were related to temporal regions as previously reported from both individuals with first-episode psychosis and individuals at clinically high risk (Korda et al., 2022). Given the association between tissue complexity and both dendritic arborization and synapse formation (Neil et al., 1998), a reduction in brain complexity observed in patients with schizophrenia had been proposed as a potential deficit of cortical maturation (Li et al., 2016).

Our findings also revealed an additional pattern of increased Lambda values, indicating enhanced brain complexity in patients, particularly in the left middle occipital gyrus, left fusiform gyrus, left thalamus, left temporal gyrus, and left cerebellum. The finding underlined the notion that in early states brain complexity was not just reduced, as had been reported for different types of dementia (Nicastro et al., 2020; Moller et al., 2016). This was consistent with our previous study (Korda et al., 2022) that first-episode psychosis or even clinical high-risk showed a generally lower pattern of Lambda values but some specific brain regions showed higher Lambda values in the left middle occipital gyrus, left temporal gyrus, left fusiform gyrus, and cerebellar regions when compared with HC. These findings suggested a redistribution of brain complexity during the early stages of schizophrenia, with potential progression as the illness advances. This was evidenced by our observation of longer DUP being associated with higher brain complexity in bilateral temporal gyri, left occipital gyrus, and cerebellum. Thus, this constellation of bidirectional findings supported a model of redistribution of brain complexity across the whole brain in schizophrenia as has been concluded from a previous functional MRI study of temporal brain entropy (another kind of complexity measure) (Xue et al., 2019). We also found that stronger expression of negative symptoms was associated with increased brain complexity in the bilateral temporal gyri, left occipital gyrus, and cerebellum. Notably, these regions partially overlapped with those associated with DUP. This observation aligned with a previous study that suggested brain structural alterations related to schizophrenia appear characterized by a "dys-structure" pattern which might mirror the psychopathological characteristics of specific clinical syndromes (Kay et al., 1987).

Applying exploratory VBM analysis to our sample, only limited GMV decrease was found in the left parahippocampus, left cerebellum crus 1, and right lingual gyrus. The decrease in hippocampal volume had been consistently reported in previous studies (Lieberman et al., 2018; van Erp et al., 2016). The decreased cerebellar regions were suggested to partly explain the cognitive impairment and motor function deficits in patients in our previous *meta*-analysis (Li et al., 2022). It was of note that decreased GMV in brain regions would deteriorate and spread to connected areas with disorder progression (Chopra et al., 2023). The antipsychotic medication would affect GMV as well (Tang et al., 2024). Compared with the VBM findings, the Chaos analysis approach based on the measurement of Lambda revealed a more widespread decrease in brain complexity at the voxel-wise level. Notably, the Lambda measure represented a "template-free" or "path-free" measurement that captured the divergence of neighboring voxels across GM topology in relation to other entitled voxels. This illustrated how voxels from distinct regions were associated with structural alternations in schizophrenia (Korda et al., 2022) and suggested that applying Lambda represented a more sensitive approach for detecting brain alternations.

Furthermore, the Lambda series was transformed into a two-dimensional scalogram using CWT to depict the brain's structural relief of brain and spatial-scale features. This enabled the quantification of cortical folding complexity, which had previously shown a regional decrease in the right superior temporal gyrus (Trevisana et al., 2022). The widespread voxel-wise decrease in Lambda components at 400

Table 4
Brain regions showing FDR-corrected decreased cortical folding complexity in FES compared with HC by applying two sample t-tests on the scalograms.

Brain regions	Number of voxels	Number of non-zero voxels	Fraction of non-zero voxels	Mean Lambda values in frequency domain of non-zero voxels
Precentral L	28,174	1	0.000	0.012
Frontal Sup Orb L	7654	12	0.002	0.033
Frontal Mid Orb L	7112	4	0.001	0.047
Frontal Inf Oper L	8271	20	0.002	0.036
Frontal Inf Tri L	20,104	13	0.001	0.042
Rolandic Oper L	7939	11	0.001	0.034
Rectus L	6864	11	0.002	0.026
Insula L	15,025	8	0.001	0.043
Cingulum Post L	3715	1	0.000	0.027
Hippocampus L	7469	25	0.003	0.024
ParaHippocampal L	7891	12	0.002	0.030
ParaHippocampal R	9028	7	0.001	0.034
Calcarine L	18,157	486	0.027	0.026
Calcarine R	14,885	202	0.014	0.022
Cuneus L	12,133	149	0.012	0.027
Cuneus R	11,323	96	0.008	0.028
Lingual L	16,932	526	0.031	0.023
Lingual R	18,450	253	0.014	0.026
Occipital Sup L	10,791	95	0.009	0.024
Occipital Sup R	11,149	78	0.007	0.020
Occipital Mid L	25,989	1944	0.075	0.022
Occipital Mid R	16,512	94	0.006	0.028
Occipital Inf L	7536	447	0.059	0.023
Occipital Inf R	7929	254	0.032	0.029
Fusiform L	18,333	850	0.046	0.022
Fusiform R	20,227	121	0.006	0.025
Postcentral L	31,053	46	0.001	0.031
Parietal Sup L	16,519	2	0.000	0.043
Parietal Inf L	19,447	52	0.003	0.037
SupraMarginal L	9907	236	0.024	0.029
Angular L	9313	230	0.025	0.028
Angular R	14,009	5	0.000	0.029
Precuneus L	28,358	84	0.003	0.032
Precuneus R	26,083	140	0.005	0.030
Caudate L	7682	1	0.000	0.035
Putamen L	7942	67	0.008	0.023
Putamen R	8510	4	0.000	0.008
Pallidum L	2285	15	0.007	0.019
Pallidum R	2188	1	0.000	0.031
Thalamus L	8700	319	0.037	0.019
Thalamus R	8399	173	0.021	0.020
Heschl L	1804	1	0.001	0.027
Temporal Sup L	18,307	305	0.017	0.028
Temporal Pole Sup L	10,228	43	0.004	0.028
Temporal Mid L	39,353	1815	0.046	0.023
Temporal Mid R	35,484	95	0.003	0.024
Temporal Pole Mid L	5984	4	0.001	0.031
Temporal Inf L	25,647	1330	0.052	0.020
Temporal Inf R	28,468	336	0.012	0.027
Cerebellum Crus1 L	20,667	1299	0.063	0.021
Cerebellum Crus1 R	21,017	606	0.029	0.026
Cerebellum Crus2 L	15,216	140	0.009	0.023
Cerebellum Crus2 R	17,038	64	0.004	0.029
Cerebellum 3 L	1072	6	0.006	0.031
Cerebellum 4 5 L	9034	4	0.000	0.015
Cerebellum 6 L	13,672	854	0.062	0.023
Cerebellum 6 R	14,362	241	0.017	0.028
Cerebellum 7b L	4639	10	0.002	0.030
Cerebellum 8 L	15,090	62	0.004	0.024
Cerebellum 8 R	18,345	11	0.001	0.025
Cerebellum 9 L	6924	23	0.003	0.029
Cerebellum 9 R	6462	7	0.001	0.027
Vermis 4 5	5324	22	0.004	0.031
Vermis 6	2956	100	0.034	0.018
Vermis 7	1564	39	0.025	0.022
Vermis 8	1940	24	0.012	0.024
Vermis 9	1367	4	0.003	0.031

Abbreviations: Inf, inferior; L, left; Mid, middle; Oper, operculum; Orb, orbital part; Post, posterior; R, right; Sup, superior; Tri, triangular part.

scales showed less lateralized specificity in patients, with decreased complexity of cortical folding primarily in the left frontal gyrus and bilaterally in other cortical regions. This suggested that decomposing the Lambda series into frequency components for feature extraction might diminish the lateralized feature of brain complexity. However, compared with the finding of brain regions with increased Lambda values, we observed a greater number of brain regions exhibiting an increased Lambda pattern in the frequency domain. This suggested that decomposing the Lambda series into the frequency domain might help determine the redistribution of topological complexity across the entire brain in schizophrenia. Interestingly, this approach revealed additional associations with symptom expression. Specifically, higher complexity of cortical folding in the right thalamus was associated with more severe depressive symptoms, while lower complexity of cortical folding in the left middle occipital gyrus was associated with more pronounced paranoid syndrome. Cortical complexity was suggested to develop during the pre/perinatal period, with only minor changes occurring until around the age of 20 (White et al., 2010). After this age, the measure remained stable throughout adulthood, making it a viable neurodevelopmental biomarker representing late fetal/early postnatal life (White et al., 2010). Based on the above, our findings further supported the neurodevelopmental hypothesis and suggested that alternations in cortical folding complexity could be considered an imaging marker of schizophrenia (Schmitt et al., 2021).

In our exploratory analysis of the gyrification index, a significant hypo-gyrification pattern in the left middle temporal and right superior temporal gyri was reported in patients with FES compared with HC. Abnormal cortical folding had been reported as a marker of aberrant fetal development in schizophrenia (Palaniyappan et al., 2013). Reduced gyrification in the temporal, precentral, precuneus (Nesvåg et al., 2014), and limbic regions (Gao et al., 2023) had been observed in both first-episode and chronic patients with schizophrenia in previous studies. Indeed, hyper-gyrification had also been reported in first-episode patients with schizophrenia, though in regions different from the current findings, such as the bilateral prefrontal and right occipital cortices (Takayanagi et al., 2019). It was notable that variation trends in cortical gyrification remained inconsistent across studies and might depend on the age and stage of illness of the recruited patients (Rosa et al., 2021). The new approach revealed a more widespread decrease in cortical complexity at a voxel-wise level. This suggested that Lambda values and their components were more sensitive in detecting cortical alterations. The finding that alterations in both hypo- and hyper-complexity were related to the same brain regions further suggested that the voxel-level approach could provide more relevant and widespread information on alternations in cortical complexity than other approaches, such as regions of interest analyses based on predefined atlases. This model was supported by previous studies showing that brain abnormalities related to schizophrenia should be rather treated as brain network alterations accounted at a voxel-level (Korda et al., 2022).

Several limitations need to be addressed. First, the Chaos analysis approach involves several parameter selections that require further

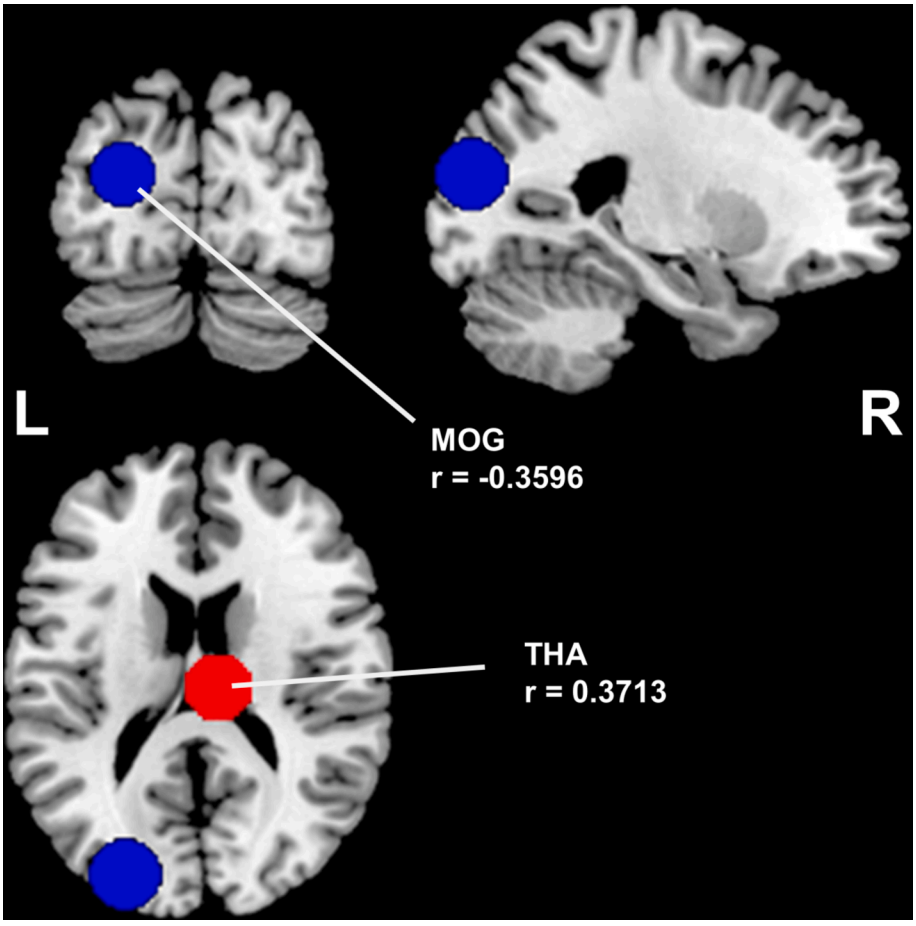

Fig. 5. Correlations between clinical symptoms and cortical folding complexity among brain regions in FES. The blue spot indicates negative correlation between left middle occipital gyrus and paranoid syndrome subscores. The red spot indicates positive correlation between right thalamus and depression subscores (FWHM = 8 mm). Abbreviations: L, left; MOG, middle occipital gyrus; R, right; THA, thalamus.

investigation, for instance determining the number of selected voxels. A general pattern of Lambda distributions in both FES and HC groups supports the assumption that sorting does not compromise spatial dependencies in the spatial signal and makes the application of the Largest Lyapunov Exponent feasible. Second, the drawback of selecting parameters arose from an assumption made due to computational restrictions, and efforts should be directed toward overcoming this challenge. To assess the effectiveness of the proposed method, comparisons with classical approaches, including gray matter volume and gyrification index were conducted in this study.

5. Conclusions

Following the Chaos analysis approach, the present study reported a general pattern of Lambda distributions in both antipsychotic-naïve patients with FES and HC, supporting the reliability of Lambda measures. The scattered distribution of altered topological complexities of the brain and cortical folding in patients compared with HC suggested that alternations in brain topology and cortical complexity might be accounted for at the voxel level. Additionally, bidirectional changes in certain regions highlighted the redistribution of complexity measures in schizophrenia at an early stage.

CRediT authorship contribution statement

Naici Liu: Writing – review & editing, Writing – original draft, Formal analysis, Conceptualization. **Rebekka Lencer:** Writing – review & editing, Supervision, Conceptualization. **Christina Andreou:** Methodology. **Mihai Avram:** Writing – review & editing. **Heinz Handels:** Methodology. **Wenjing Zhang:** Writing – review & editing, Funding acquisition, Conceptualization. **Sun Hui:** Writing – review & editing. **Chengmin Yang:** Writing – review & editing. **Stefan Borgwardt:** Supervision, Conceptualization. **John A. Sweeney:** Supervision. **Su Lui:** Writing – review & editing, Supervision, Funding acquisition, Conceptualization. **Alexandra I. Korda:** Writing – review & editing, Visualization, Methodology, Formal analysis, Conceptualization.

Declaration of competing interest

The authors declare that they have no known competing financial interests or personal relationships that could have appeared to influence the work reported in this paper.

Acknowledgments

This study was supported by the National Natural Science Foundation of China (Project Nos. 8212018014, 82071908, and 82101998), National Key R&D Program of China (Project Nos. 2022YFC2009901 and 2022YFC2009900), Chengdu Science and Technology Office, major technology application demonstration project (Project No. 2022-YF09-00062-SN, 2022-GH03-00017-HZ), Sichuan Science and Technology Program (Project Nos. 2021JDTD0002), 1.3.5 project for disciplines of excellence, West China Hospital, Sichuan University (Project Nos. ZYGD23003 , ZYAI24010), and the Fundamental Research Funds for the Central Universities (Project No. ZYGX2022YGRH008). Dr. Su Lui acknowledges the support from Humboldt Foundation Friedrich

Wilhelm Bessel Research Award and Chang Jiang Scholars (Program No. T2019069).

Disclosures

Drs. John A. Sweeney and Wenjing Zhang consult to VeraSci. The remaining authors have no competing interests or financial support to disclose.

Appendix A. Supplementary data

Supplementary data to this article can be found online at https://doi.org/10.1016/j.nicl.2024.103686.

Data availability

Data will be made available on request.

References

Breakspear, M., 2006. The nonlinear theory of schizophrenia. Aust. N. Z. J. Psychiatry 40 (1), 20–35.

Chen, Y., Pham, T.D., 2013. Sample entropy and regularity dimension in complexity analysis of cortical surface structure in early Alzheimer's disease and aging. J. Neurosci. Methods 215 (2), 210–217.

Chopra, S., Segal, A., Oldham, S., Holmes, A., Sabaroedin, K., Orchard, E.R., et al., 2023. Network-based spreading of gray matter changes across different stages of psychosis. JAMA Psychiat. 80 (12), 1246–1257.

Cuadra, M.B., Cammoun, L., Butz, T., Cuisenaire, O., Thiran, J.P., 2005. Comparison and validation of tissue modelization and statistical classification methods in T1-weighted MR brain images. IEEE Trans. Med. Imaging 24 (12), 1548–1565.

Dahnke, R., Yotter, R.A., Gaser, C., 2013. Cortical thickness and central surface estimation. Neuroimage 65, 336–348.

Dragovic, M., Hammond, G., 2007. A classification of handedness using the annett hand preference questionnaire. Brit. J. Psychol. 98, 375–387.

Fernandez, A., Gomez, C., Hornero, R., Lopez-Ibor, J.J., 2013. Complexity and schizophrenia. Prog. Neuropsychopharmacol. Biol. Psychiatry 45, 267–276.

First, M.B.J., 2002. Structured clinical interview for DSM-IV-TR axis I disorders, research version, non-patient edition (SCID-I/NP).

First, M.B.J., 2005. Structured clinical interview for DSM-IV-TR axis I disorders.

Fornito, A., Yucel, M., Patti, J., Wood, S.J., Pantelis, C., 2009. Mapping grey matter reductions in schizophrenia: an anatomical likelihood estimation analysis of voxel-based morphometry studies. Schizophr. Res. 108 (1–3), 104–113.

Fornito, A., Zalesky, A., Pantelis, C., Bullmore, E.T., 2012. Schizophrenia, neuroimaging and connectomics. Neuroimage 62 (4), 2296–2314.

Gao, X., Yao, L., Li, F., Yang, C., Zhu, F., Gong, Q., et al., 2023. The cortical hypogyrification pattern in antipsychotic-naive first-episode schizophrenia. Cereb. Cortex 33 (12), 7619–7626.

Gladsjo, J.A., McAdams, L.A., Palmer, B.W., Moore, D.J., Jeste, D.V., Heaton, R.K., 2004. A six-factor model of cognition in schizophrenia and related psychotic disorders: relationships with clinical symptoms and functional capacity. Schizophr Bull. 30 (4), 739–754.

He, Y., Evans, A., 2010. Graph theoretical modeling of brain connectivity. Curr. Opin. Neurol. 23 (4), 341–350.

Jiang, Y., Yao, D., Zhou, J., Tan, Y., Huang, H., Wang, M., et al., 2022. Characteristics of disrupted topological organization in white matter functional connectome in schizophrenia. Psychol. Med. 52 (7), 1333–1343.

Kay, S.R., Fiszbein, A., Opler, L.A., 1987. The positive and negative syndrome scale (Panss) for schizophrenia. Schizophrenia Bull. 13 (2), 261–276.

Kim, D.J., Jeong, J., Chae, J.H., Park, S., Yong Kim, S., Jin Go, H., et al., 2000. An estimation of the first positive Lyapunov exponent of the EEG in patients with schizophrenia. Psychiatry Res. 98 (3), 177–189.

Kim, J.H., Son, Y.D., Kim, J.H., Choi, E.J., Lee, S.Y., Lee, J.E., et al., 2015. Serotonin transporter availability in thalamic subregions in schizophrenia: a study using 7.0-T MRI with [(11)C]DASB high-resolution PET. Psychiatry Res. 231 (1), 50–57.

Koelkebeck, K., Miyata, J., Kubota, M., Kohl, W., Son, S., Fukuyama, H., et al., 2014. The contribution of cortical thickness and surface area to gray matter asymmetries in the healthy human brain. Hum. Brain Mapp. 35 (12), 6011–6022.

Kong, X.Z., Mathias, S.R., Guadalupe, T., Glahn, D.C., Franke, B., Crivello, F., et al., 2018. Mapping cortical brain asymmetry in 17,141 healthy individuals worldwide via the ENIGMA Consortium. Proc. Natl. Acad. Sci. U.S.A. 115 (22), E5154–E5163.

Korda, A.I., Asvestas, P.A., Matsopoulos, G.K., Ventouras, E.M., Smyrnis, N., 2018. Automatic identification of eye movements using the largest lyapunov exponent. Biomed. Signal Process. 41, 10–20.

Korda, A.I., Andreou, C., Avram, M., Handels, H., Martinetz, T., Borgwardt, S., 2022. Chaos analysis of the brain topology in first-episode psychosis and clinical high risk patients. Front. Psychiatry 13.

Korda, A.I., Ventouras, E., Asvestas, P., Toumaian, M., Matsopoulos, G.K., Smyrnis, N., 2022. Convolutional neural network propagation on electroencephalographic scalograms for detection of schizophrenia. Clin. Neurophysiol. 139, 90–105.

Li, X., Liu, N.C., Yang, C.M., Zhang, W.J., Lui, S., 2022. Cerebellar gray matter volume changes in patients with schizophrenia: a voxel-based meta-analysis. Front. Psychiatry 13.

Li, Y., Xie, S., Liu, B., Song, M., Chen, Y., Li, P., et al., 2016. Diffusion magnetic resonance imaging study of schizophrenia in the context of abnormal neurodevelopment using multiple site data in a Chinese Han population. Transl. Psychiat. 6.

Lieberman, J.A., Girgis, R.R., Brucato, G., Moore, H., Provenzano, F., Kegeles, L., et al., 2018. Hippocampal dysfunction in the pathophysiology of schizophrenia: a selective review and hypothesis for early detection and intervention. Mol. Psychiatr. 23 (8), 1764–1772.

Liu, Z.W., Palaniyappan, L., Wu, X.R., Zhang, K., Du, J.N., Zhao, Q., et al., 2021. Resolving heterogeneity in schizophrenia through a novel systems approach to brain structure: individualized structural covariance network analysis. Mol. Psychiatr. 26 (12), 7719–7731.

Luders, E., Thompson, P.M., Narr, K.L., Toga, A.W., Jancke, L., Gaser, C., 2006. A curvature-based approach to estimate local gyrification on the cortical surface. Neuroimage 29 (4), 1224–1230.

Moller, C., Hafkemeijer, A., Pijnenburg, Y.A.L., Rombouts, S., van der Grond, J., Dopper, E., et al., 2016. Different patterns of cortical gray matter loss over time in behavioral variant frontotemporal dementia and Alzheimer's disease. Neurobiol. Aging 38, 21–31.

Neil, J.J., Shiran, S.I., McKinstry, R.C., Schefft, G.L., Snyder, A.Z., Almli, C.R., et al., 1998. Normal brain in human newborns: apparent diffusion coefficient and diffusion anisotropy measured by using diffusion tensor MR imaging. Radiology 209 (1), 57–66.

Nesvåg, R., Schaer, M., Haukvik, U.K., Westlye, L.T., Rimol, L.M., Lange, E.H., et al., 2014. Reduced brain cortical folding in schizophrenia revealed in two independent samples. Schizophr. Res. 152 (2–3), 333–338.

Nicastro, N., Malpetti, M., Cope, T.E., Bevan-Jones, W.R., Mak, E., Passamonti, L., et al., 2020. Cortical complexity analyses and their cognitive correlate in Alzheimer's disease and frontotemporal dementia. J. Alzheimers Dis. 76 (1), 331–340.

Palaniyappan, L., Marques, T.R., Taylor, H., Handley, R., Mondelli, V., Bonaccorso, S., et al., 2013. Cortical folding defects as markers of poor treatment response in first-episode psychosis. JAMA Psychiat. 70 (10), 1031–1040.

Palaniyappan, L., Park, B., Balain, V., Dangi, R., Liddle, P., 2015. Abnormalities in structural covariance of cortical gyrification in schizophrenia. Brain Struct. Funct. 220 (4), 2059–2071.

Pham, T.D., Abe, T., Oka, R., Chen, Y.F., 2015. Measures of morphological complexity of gray matter on magnetic resonance imaging for control age grouping. Entropy 17 (12), 8130–8151.

Rand, D.A., Young, L.-S., (Eds.), 1981. Dynamical Systems and Turbulence, Warwick 1980.

Rosa, P.G.P., Zugman, A., Cerqueira, C.T., Serpa, M.H., de Souza Duran, F.L., Zanetti, M. V., et al., 2021. Cortical surface abnormalities are different depending on the stage of schizophrenia: a cross-sectional vertexwise mega-analysis of thickness, area and gyrification. Schizophr. Res. 236, 104–114.

Rosenstein, M.T., Collins, J.J., De Luca, C.J., 1993. A practical method for calculating largest lyapunov exponents from small data sets. Physica D 65 (1–2), 117–134.

Schijven, D., Postema, M.C., Fukunaga, M., Matsumoto, J., Miura, K., de Zwarte, S.M.C., et al., 2023. Large-scale analysis of structural brain asymmetries in schizophrenia via the ENIGMA consortium. PNAS 120 (14), e2213880120.

Schmitt, S., Meller, T., Stein, F., Brosch, K., Ringwald, K., Pfarr, J.K., et al., 2021. Effects of polygenic risk for major mental disorders and cross-disorder on cortical complexity. Psychol. Med. 52 (16), 1–12.

Sha, Z., Schijven, D., Francks, C., 2021. Patterns of brain asymmetry associated with polygenic risks for autism and schizophrenia implicate language and executive functions but not brain masculinization. Mol. Psychiatry 26 (12), 7652–7660.

Singh, S.P., Cooper, J.E., Fisher, H.L., Tarrant, C.J., Lloyd, T., Banjo, J., et al., 2005. Determining the chronology and components of psychosis onset: the Nottingham Onset Schedule (NOS). Schizophr. Res. 80 (1), 117–130.

Spalthoff, R., Gaser, C., Nenadic, I., 2018. Altered gyrification in schizophrenia and its relation to other morphometric markers. Schizophr. Res. 202, 195–202.

Spreng, R.N., DuPre, E., Ji, J.L., Yang, G., Diehl, C., Murray, J.D., et al., 2019. Structural covariance reveals alterations in control and salience network integrity in chronic schizophrenia. Cereb. Cortex 29 (12), 5269–5284.

Squarcina, L., De Luca, A., Bellani, M., Brambilla, P., Turkheimer, F.E., Bertoldo, A., 2015. Fractal analysis of MRI data for the characterization of patients with schizophrenia and bipolar disorder. Phys. Med. Biol. 60 (4), 1697–1716.

Takayanagi, Y., Sasabayashi, D., Takahashi, T., Komori, Y., Furuichi, A., Kido, M., et al., 2019. Altered brain gyrification in deficit and non-deficit schizophrenia. Psychol. Med. 49 (4), 573–580.

Tang, Y.L., Li, Y.T., Cao, P.Y., Dong, Y.B., Xu, G.X., Si, Q., et al., 2024. Striatum and globus pallidus structural abnormalities in schizophrenia: a retrospective study of the different stages of the disease. Prog. Neuro-Psychoph. 133.

Tian, Y., Zalesky, A., Bousman, C., Everall, I., Pantelis, C., 2019. Insula functional connectivity in schizophrenia: subregions, gradients, and symptoms. Biol. Psychiatry Cogn. Neurosci. Neuroimaging 4 (4), 399–408.

Toga, A.W., Thompson, P.M., 2003. Mapping brain asymmetry. Nat. Rev. Neurosci. 4 (1), 37–48.

Trevisana, N., Miola, A., Cattarinussi, G., Kubera, K.M., Hirjak, D., Wolf, R.C., et al., 2022. Cortical folding complexity is distinctively altered in schizophrenia and bipolar disorder. Schizophr. Res. 241, 92–93.

van den Heuvel, M.P., Fornito, A., 2014. Brain networks in schizophrenia. Neuropsychol. Rev. 24 (1), 32–48.

van den Heuvel, M.P., Stam, C.J., Boersma, M., Hulshoff Pol, H.E., 2008. Small-world and scale-free organization of voxel-based resting-state functional connectivity in the human brain. Neuroimage 43 (3), 528–539.
van Erp, T.G.M., Hibar, D.P., Rasmussen, J.M., Glahn, D.C., Pearlson, G.D., Andreassen, O.A., et al., 2016. Subcortical brain volume abnormalities in 2028 individuals with schizophrenia and 2540 healthy controls via the ENIGMA consortium. Mol. Psychiatr. 21 (4), 547–553.
White, T., Su, S., Schmidt, M., Kao, C.Y., Sapiro, G., 2010. The development of gyrification in childhood and adolescence. Brain Cogn. 72 (1), 36–45.
Xue, S.W., Yu, Q., Guo, Y., Song, D., Wang, Z., 2019. Resting-state brain entropy in schizophrenia. Compr. Psychiatry 89, 16–21.
Yu, Q.B., Du, Y.H., Chen, J.Y., Sui, J., Adali, T., Pearlson, G.D., et al., 2018. Application of graph theory to assess static and dynamic brain connectivity: approaches for building brain graphs. Proc. IEEE 106 (5), 886–906.
Zhang, W.J., Lei, D., Keedy, S.K., Ivleva, E.I., Eum, S., Yao, L., et al., 2020. Brain gray matter network organization in psychotic disorders. Neuropsychopharmacology 45 (4), 666–674.
Zhang, W., Sweeney, J.A., Bishop, J.R., Gong, Q., Lui, S., 2023. Biological subtyping of psychiatric syndromes as a pathway for advances in drug discovery and personalized medicine. Nat. Mental Health 1 (2), 88–99.